IEEE TRANSACTIONS ON COMMUNICATIONS, VOL. XX, NO. XX, XXX 2023

Automatic Identification of Space-Time Block Coding for MIMO-OFDM Systems in the Presence of Impulsive Interference

Junlin Zhang, Mingqian Liu, *Member, IEEE*, Yunfei Chen, *Senior Member, IEEE*, Nan Zhao, *Senior Member, IEEE*, and Arumugam Nallanathan, *Fellow, IEEE*

***Abstract*—Signal identification, a vital task of intelligent communication radios, finds its applications in various military and civil communication systems. Previous works on identification for space-time block codes (STBC) of multiple-input multiple-output (MIMO) system employing orthogonal frequency division multiplexing (OFDM) are limited to additive white Gaussian noise. In this paper, we develop a novel automatic identification algorithm to exploit the generalized cross-correntropy function of the received signals to classify STBC-OFDM signals in the presence of Gaussian noise and impulsive interference. This algorithm first introduces the generalized cross-correntropy function to fully utilize the space-time redundancy of STBC-OFDM signals. The strongly-distinguishable discriminating matrix is then constructed by using the generalized cross-correntropy for multiple receive antennas. Finally, a decision tree identification algorithm is employed to identify the STBC-OFDM signals which is extended by the binary hypothesis test. The proposed algorithm avoids the traditionally required pre-processing tasks, such as channel coefficient estimation, noise and interference statistics prediction and modulation type recognition. Numerical results are presented to show that the proposed scheme provides good identification performance by exploiting the generalized cross-correntropy function of STBC-OFDM signals under impulsive interference circumstances.**

***Index Terms*—Impulsive interference, multiple-input multiple-output, orthogonal frequency division multiplexing, signal identification, space-time block code.**

I. Introduction

SIGNAL identification is the primary task of identifying the transmission parameters of communication signals with minimal requirements for a priori knowledge. It allows a variety of applications in intelligent wireless communication systems, such as software-defined and cognitive radios [1], [2]. In the context of software-defined radio systems, a flexible hardware platform under software control permits the transmitter to choose transmission parameters, such as modulation type and coding rate [3], [4]. At the receiving terminal, signal identification is required to determine transmission parameters of communication signals subject to impairments. Moreover, cognitive radio systems takes sensing spectrum state and identifying existing signals as a major task to achieve transmission with acceptable interference [5], [6]. A considerable amount of literature has been conducted for efficient and applicable methods of signal identification for single-input single-output systems. However, the advent and rapid adoption of multiple-input-multiple-output with space-time block coding (STBC) presents new signal parameters to discriminate and new challenges to conquer, such as the detection of transmit-antennas number and STBC identification under complicated circumstances [7]–[9].

Several previous investigations on STBC identification has reported for multiple-input multiple-output with single-carrier (MIMO-SC). Two commonly used algorithms are likelihood-based (LB) and feature-based (FB) methods for MIMO-SC. The former computes the conditional probability density function of the received signal for multiple hypotheses and then utilizes the likelihood ratio test to discriminate between several STBCs. In [10], Choqueuse *et al*. proposed three new maximum-likelihood (ML) based schemes to classify STBC format, namely the optimal classifier, second-order statistic (SOS) classifier and code parameter (CP) classifier. The optimal and the SOS algorithms exhibit an acceptable classification performance, but they assume ideal conditions. The CP classifier performs well in the absence of prior knowledge. Marey *et al*. in [11] developed a maximum-likelihood-based scheme to recognize the STBC signals and modulation formats. For the FB approach, the space-time redundancy of the received signals is employed to construct a discriminating feature for classifying STBCs. Choqueuse *et al*. in [12] presented an algorithm relying on the Frobenius norms of the space-time correlations. This algorithm exhibits a good performance at low signal-to-noise ratios, but it assumes a perfect estimate of timing synchronization. In [13], a maximum-likelihood criterion-based classification algorithm and a false alarm rate-based classification algorithm were presented by exploiting the cross-correlation properties of the STBC signals. These two schemes achieve a good classification performance and avoid the need for a modulation format. Yahia *et al*. in [14] designed a likelihood ratio algorithm relying upon the fourth-order moment and three classification algorithms exploiting the fourth-order lag product (FOLP) to distinguish

J. Zhang and M. Liu are with the State Key Laboratory of Integrated Service Networks, Xidian University, Shaanxi, Xi'an 710071, China , and also with the Collaborative Innovation Center of Information Sensing and Understanding, Xidian University, Shaanxi, Xi'an 710071, China (e-mail: zhangjunlin@xidian.edu.cn; mqliu@mail.xidian.edu.cn).

Y. Chen is with Department of Engineering, University of Durham, Durham, UK DH1 3LE (e-mail: Yunfei.Chen@durham.ac.uk).

N. Zhao is with the School of Information and Communication Engineering, Dalian University of Technology, Dalian 116024, China (e-mail: zhaonan@dlut.edu.cn).

A. Nallanathan is with the School of Electronic Engineering and Computer Science, Queen Mary University of London, London E1 4NS, U.K. (e-mail: a.nallanathan@qmul.ac.uk)

STBC signals. The first algorithm requires the prior knowledge of signal parameters, but three FOLP-based algorithms overcome this drawback. Shi *et al*. developed a classification scheme based on the cyclic correlations introduced by the space-time redundancy to distinguish STBC from Bell Labs Layered Space Time Architecture in [15]. In [16], Marey *et al*. exploited the second-order cyclic statistics of STBC signals as the discriminating feature and proposed a cyclostationarity-based classification algorithm in the presence of transmission impairments. Mohammadkarimi *et al*. in [17] formulated the signal identification problem as a goodness of fit test and employed the Kolmogorov-Smirnov test to classify spatial multiplexing (SM) and Alamouti (AL) space-time block code. This algorithm provides a good performance and requires little prior information on signal parameters.

STBC identification for multiple-input multiple-output-orthogonal frequency division multiplexing (MIMO-OFDM) systems has received relatively less attention in the field of signal identification than MIMO-SC. Existing works devoted to STBC identification for MIMO-OFDM mainly follow the FB approach. In [18], Marey *et al*. presented a new hypothesis test-based method to identify STBC-OFDM signals by investigating the cross-correlation of the received signals from different antennas. While the method is sensitive to frequency offset, it does not require a priori information of transmission parameters. Eldemerdash *et al*. in [19] developed an efficient scheme to blindly the SM and AL codes for MIMO-OFDM systems. A novel cross-correlation of received signals is introduced to provide an efficient feature for STBC-OFDM identification. In [20], Karami *et al*. focused on the application of second-order cyclostationarity properties to blindly identify the SM-OFDM and AL-OFDM signals. These algorithms in [19] and [20] achieve a satisfactory performance with a shorter observation time, and they are robust to the carrier frequency offset. In [21], Marey *et al*. designed STBC identification and channel estimation scheme for OFDM transmissions. However, all these works considered only the Gaussian noise assumption. In practice, impulsive interference caused by man-made and natural noise consistently occurs in wireless channels [22], [23]. The α-stable distribution provides an efficient solution to model non-Gaussian impulsive behavior. Unfortunately, the STBC-OFDM identification algorithms designed for Gaussian noise do not perform well in non-Gaussian interference. In the literature, several solutions have been suggested to ameliorate the performance of signal identification for SISO systems in the presence of non-Gaussian noise/interference [24], [25]. Terms from the existing literature and investigations, there has been no work involving the automatic identification of STBC for MIMO-OFDM systems in the presence of Gaussian noise and impulsive interference.

In this paper, we present an efficient algorithm aimed at identifying the STBC-OFDM signals corrupted by impulsive interference in frequency-selective fading channels. A novel generalized cross-correntropy is introduced for the received signals, which provides a powerful discriminating feature. Using this, a novel decision tree algorithm is developed. The proposed algorithm does not require prior information of the signal and channel parameters. Moreover, it has the advantage of providing a good identification performance under the Gaussian noise and impulsive interference. The main contributions of this paper are summarized as follows.

- Unlike previous works considering the Gaussian noise only, we investigate the efficient identification algorithm for STBC-OFDM signals corrupted by both the impulsive interference and Gaussian noise. We assume that impulsive interference follows a symmetric alpha-stable distribution. The space-time code candidate pool of four linear STBCs (SM, AL, STBC3, and STBC4) is considered.
- The generalized cross-correntropy function between receive antenna pairs is introduced to take full advantage of space-time redundancy for STBC-OFDM signals. Then, a decision tree algorithm is proposed to improve the identification performance in Gaussian noise and impulsive interference over frequency-selective fading channels. The identification algorithm based on generalized cross-correntropy function does not need accurate information about the channel knowledge, the number of transmit antennas, modulation type, and signal-to-noise/interference ratio.
- The performance of the proposed identification algorithm is also evaluated in the context of different system parameters. The experimental result indicated that the identification algorithm achieves a satisfactory identification performance with symmetric alpha stable interference

TABLE I
NOTATIONS.

Notations	Descriptions	Notations	Descriptions
$[\cdot]^{\mathrm{T}}$	Transposition	$\lvert\cdot\rvert$	Absolute value
mod	Modulo operation	$(\cdot)^*$	Complex conjugate
$E\{\cdot\}$	Mathematical expectation	U^{λ}	Block length of STBC
x^f	The symbol x at the f-th antenna	$G^{(i_l,i_k)}$	The variable G depend on antenna i_l and i_k
$\exp(\cdot)$	Exponential function	$\lVert\cdot\rVert_{\mathrm{F}}$	Frobenius norm
δ	Kronecker delta	$\Gamma(\cdot)$	Gamma Function
$\lVert\cdot\rVert_{l_1}$	l_1 norm	$\lVert\cdot\rVert_{l_2}$	l_2 norm
$\Pr(\mathrm{C})$	Probability of the event C	$\approx$	Approximately equal sign

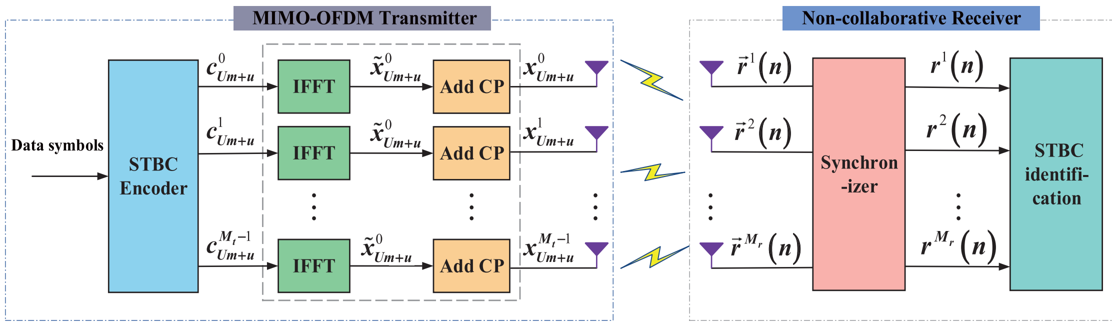

Fig. 1. Block diagram of the STBC identification for MIMO-OFDM systems.

in the moderate-to-high SNR range, and is robust with respect to the characteristic exponent.

The remainder of this paper is organized as follows. Section II defines the system model. Section III presents the generalized cross-correntropy function of different STBCs and describes a decision tree identification algorithm for STBC-OFDM signals. The simulation results are provided in Section IV. Finally, this paper is summarized in Section V. Table I lists the notations used in this paper.

II. System Model

Consider a wireless MIMO-OFDM systems with M_t transmit antennas and M_r receive antennas, which employs an STBC architecture as shown in Fig 1. Assuming that the transmission data symbols are random and independent, and drawn from either an M-ary quadrature amplitude modulation (QAM) or phase-shift keying (PSK) signal constellation. The modulated data stream is parsed into data blocks of length N_z. The STBC encoder employs a code matrix $\mathbf{C}(\{\mathbf{d}_m\})$ of size $M_t \times N_z U$ to encode each data block $\{\mathbf{d}_m\}$ to be transmitted during U block instants. In this paper, the codewords include SM, AL, and two STBCs with different code rates [18], [26], whose codeword matrices are given by

$$\begin{aligned}\mathbf{C}^{\mathrm{SM}} &= \begin{bmatrix} \mathbf{c}^0_{m+0} & \mathbf{c}^1_{m+0} \end{bmatrix} \\ &= \begin{bmatrix} \mathbf{d}_{2m+0} & \mathbf{d}_{2m+1} \end{bmatrix},\end{aligned} \tag{1}$$

$$\begin{aligned}\mathbf{C}^{\mathrm{AL}} &= \begin{bmatrix} \mathbf{c}^0_{2m+0} & \mathbf{c}^1_{2m+0} \\ \mathbf{c}^0_{2m+1} & \mathbf{c}^1_{2m+1} \end{bmatrix} \\ &= \begin{bmatrix} \mathbf{d}_{2m+0} & \mathbf{d}_{2m+1} \\ -\mathbf{d}^*_{2m+1} & \mathbf{d}^*_{2m+0} \end{bmatrix},\end{aligned} \tag{2}$$

$$\begin{aligned}\mathbf{C}^{\mathrm{STBC3}} &= \begin{bmatrix} \mathbf{c}^0_{4m+0} & \mathbf{c}^1_{4m+0} & \mathbf{c}^2_{4m+0} \\ \mathbf{c}^0_{4m+1} & \mathbf{c}^1_{4m+1} & \mathbf{c}^2_{4m+1} \\ \mathbf{c}^0_{4m+2} & \mathbf{c}^1_{4m+2} & \mathbf{c}^2_{4m+2} \\ \mathbf{c}^0_{4m+3} & \mathbf{c}^1_{4m+3} & \mathbf{c}^2_{4m+3} \end{bmatrix} \\ &= \begin{bmatrix} \mathbf{d}_{3m+0} & \mathbf{d}_{3m+1} & \mathbf{d}_{3m+2} \\ -\mathbf{d}^*_{3m+1} & \mathbf{d}^*_{3m+0} & \mathbf{0} \\ -\mathbf{d}^*_{3m+2} & \mathbf{0} & \mathbf{d}^*_{3m+0} \\ \mathbf{0} & -\mathbf{d}^*_{3m+2} & \mathbf{d}^*_{3m+1} \end{bmatrix},\end{aligned} \tag{3}$$

$$\begin{aligned}\mathbf{C}^{\mathrm{STBC4}} &= \begin{bmatrix} \mathbf{c}^0_{8m+0} & \mathbf{c}^1_{8m+0} & \mathbf{c}^2_{8m+0} \\ \mathbf{c}^0_{8m+1} & \mathbf{c}^1_{8m+1} & \mathbf{c}^2_{8m+1} \\ \mathbf{c}^0_{8m+2} & \mathbf{c}^1_{8m+2} & \mathbf{c}^2_{8m+2} \\ \mathbf{c}^0_{8m+3} & \mathbf{c}^1_{8m+3} & \mathbf{c}^2_{8m+3} \\ \mathbf{c}^0_{8m+4} & \mathbf{c}^1_{8m+4} & \mathbf{c}^2_{8m+4} \\ \mathbf{c}^0_{8m+5} & \mathbf{c}^1_{8m+5} & \mathbf{c}^2_{8m+5} \\ \mathbf{c}^0_{8m+6} & \mathbf{c}^1_{8m+6} & \mathbf{c}^2_{8m+6} \\ \mathbf{c}^0_{8m+7} & \mathbf{c}^1_{8m+7} & \mathbf{c}^2_{8m+7} \end{bmatrix} \\ &= \begin{bmatrix} \mathbf{d}_{4m+0} & \mathbf{d}_{4m+1} & \mathbf{d}_{4m+2} \\ -\mathbf{d}_{4m+1} & \mathbf{d}_{4m+0} & -\mathbf{d}_{4m+3} \\ -\mathbf{d}_{4m+2} & \mathbf{d}_{4m+3} & \mathbf{d}_{4m+0} \\ -\mathbf{d}_{4m+3} & -\mathbf{d}_{4m+2} & \mathbf{d}_{4m+1} \\ \mathbf{d}^*_{4m+0} & \mathbf{d}^*_{4m+1} & \mathbf{d}^*_{4m+2} \\ -\mathbf{d}^*_{4m+1} & \mathbf{d}^*_{4m+0} & -\mathbf{d}^*_{4m+3} \\ -\mathbf{d}^*_{4m+2} & \mathbf{d}^*_{4m+3} & \mathbf{d}^*_{4m+0} \\ -\mathbf{d}^*_{4m+3} & -\mathbf{d}^*_{4m+2} & \mathbf{d}^*_{4m+0} \end{bmatrix}.\end{aligned} \tag{4}$$

The output of the encoder $\mathbf{c}^f_{Um+u}$ is fed into an N_z-point inverse fast Fourier transform, yielding the time-domain block $\tilde{\mathbf{x}}^f_{Um+u} = \left[\tilde{x}^f_{Um+u}(0), \tilde{x}^f_{Um+u}(1), \cdots, \tilde{x}^f_{Um+u}(N_z-1)\right]$.

Subsequently, the last ν samples are appended as a cyclic prefix, with the resulting OFDM symbol given by $\mathbf{x}^f_{Um+u} = \left[x^f_{Um+u}(0), x^f_{Um+u}(\nu), \cdots, x^f_{Um+u}(N_z+\nu-1)\right]$. Hence, the OFDM block can be expressed as

$$x^f_{Um+u}(n_1)=\frac{1}{\sqrt{N_z}}\sum_{p=0}^{N_z-1} c^f_{Um+u}(p)\exp\left(\frac{j2\pi p(n_1-\nu)}{N_z}\right), \quad (5)$$

where $n_1 = 0, 1, \cdots, N_z+\nu-1$. Furthermore, the transmitted sequence from the f-th antenna can be written as $S^f = \left[\cdots, \mathbf{x}^f_{-2}, \mathbf{x}^f_{-1}, \mathbf{x}^f_0, \mathbf{x}^f_1, \mathbf{x}^f_2, \cdots\right]$. The transmit sequence from the f-th antenna is distorted by an unknown L_h-path frequency-selective fading channel characterized by the vector $\mathbf{h}_{fi} = \left[h_{fi}(l), \cdots, h_{fi}(L_h-1)\right]$. Accordingly, the received signal at the i-th receive antenna can be written as

$$\begin{aligned} r^i(n) &= \tilde{s}^i(n) + I^i(n) + w^i(n) \\ &= \sum_{f=0}^{M_t-1}\sum_{l=0}^{L_h-1} h_{fi}(l)\, s^f(n-l) + I^i(n) + w^i(n), \end{aligned} \quad (6)$$

where L_h is the number of propagation paths, $h_{fi}(l)$ is the channel coefficient corresponding to the l-th path between the f-th transmit antenna and the i-th receive antenna, $w^i(n)$ is the Gaussian noise with mean and variance σ_w^2 and $I^i(n)$ represents the impulsive interference at the i-th receive antenna.

The impulsive interference is modeled by the symmetric alpha stable distribution ($S\alpha S$) in this paper. $S\alpha S$ is a simplification of the alpha stable distribution that is an excellent model for impulsive interference [27]–[29]. A stable distributed random variable y is denoted as $y \sim S\alpha S(\gamma_\alpha, e_\alpha)$, which is described by its characteristic function as

$$\varphi(y) = \exp\left\{ je_\alpha y - \gamma_\alpha |y|^\alpha \right\}, \quad (7)$$

where γ_α is the dispersion coefficient, e_α is the location parameter, and α is the characteristic exponent with $1 < \alpha < 2$. Two special-case alpha distributions are the Cauchy distribution where $\alpha = 1$ and the Gaussian distribution where $\alpha = 2$.

The next section discusses the STBC identification scheme for MIMO-OFDM systems which leverages the generalized cross-correntropy to overcome the shortcomings associated with conventional identification algorithms.

III. Identification of STBC-OFDM Based on Generalized Cross-Correntropy

In this section, we first analyze the generalized cross-correntropy of the received signals from different antennas. Then, a novel identification scheme using the generalized cross-correntropy function is proposed to distinguish STBC-OFDM signals.

A. Generalized Cross-Correntropy Function

The correntropy is a generalization of the correlation function that can better suppress the impulsive noise/interference. The correntropy function and its extension recently find various applications in the field of signal processing as a novel theory and approach for statistical characteristics, such as signal detection, parameter estimation and target localization [30]–[32]. In order to tackle the impulsive interference, a novel generalized cross-correntropy is introduced to extract the discriminating feature for identifying STBC-OFDM signals, which relies on the space-time redundancy of the received signals from different antennas.

We first define the generalized cross-correntropy function between the i_1-th receive antenna and the i_2-th receive antenna as

$$\begin{aligned} &G(n, n+\tau) \\ &= \frac{1}{U^\lambda}\sum_{g=0}^{U^\lambda-1} E\left\{\kappa_\varsigma\left(r^{i_1}(n_g) - r^{i_2}(n_g+\tau_g)\right)\mathcal{J}(n_g, n_g+\tau_g)\right\}, \end{aligned} \quad (8)$$

where $n_g = n + g(N_z+\nu)$, $n_g + \tau_g = n + (g+\tau)(N_z+\nu)$ and $\mathcal{J}(n_g, n_g+\tau_g) = r^{i_1}(n_g)\, r^{i_2}(n_g+\tau_g)$. $\kappa_\varsigma\left(r^{i_1}(n_g) - r^{i_2}(n_g+\tau_g)\right)$ is expressed as in (9) at the bottom of the page, where υ is the width parameter, ς is the shape parameter and $\upsilon > 0$, $\varsigma > 0$, ξ_g is the suppression parameter and $|\vartheta|$ is a very small constant. U^λ denotes the block length of STBC and $\lambda \in \{\mathrm{SM}, \mathrm{AL}, \mathrm{STBC3}, \mathrm{STBC4}\}$.

The generalized cross-correntropy function $G_r(n, n+\tau)$

$$\kappa_\varsigma\left(r^{i_1}(n_g) - r^{i_2}(n_g+\tau_g)\right) = \frac{\varsigma}{2\upsilon\Gamma(1/\varsigma)}\exp\left(-\left|\frac{r^{i_1}(n_g) - \xi_g r^{i_2}(n_g+\tau_g) + |\vartheta|}{\upsilon}\right|^\varsigma\right) \quad (9)$$

$$\begin{aligned} G_r(n, n+\tau) &= \frac{1}{U^\lambda}\sum_{g=0}^{U^\lambda-1}\frac{\varsigma}{2\upsilon\Gamma(1/\varsigma)} E\left\{\frac{r^{i_1}(n_g)\, r^{i_2}(n_g+\tau_g)}{\Omega_\kappa}\right\} \\ &= \frac{1}{U^\lambda}\sum_{g=0}^{U^\lambda-1}\frac{\varsigma}{2\upsilon\Gamma(1/\varsigma)} E\left\{\frac{\tilde{s}^{i_1}(n_g) + I^{i_1}(n_g) + w^{i_1}(n_g)}{\Omega_\kappa}\left(\tilde{s}^{i_2}(n_g+\tau_g) + I^{i_2}(n_g+\tau_g) + w^{i_2}(n_g+\tau_g)\right)\right\} \\ &\approx \frac{1}{U^\lambda}\sum_{g=0}^{U^\lambda-1}\frac{\varsigma}{2\upsilon\Gamma(1/\varsigma)}\left(E\left\{\frac{\tilde{s}^{i_1}(n_g)\,\tilde{s}^{i_2}(n_g+\tau_g)}{\Omega_\kappa}\right\} + E\left\{\frac{I^{i_1}(n_g)\, I^{i_2}(n_g+\tau_g)}{\Omega_\kappa}\right\} + E\left\{\frac{w^{i_1}(n_g)\, w^{i_2}(n_g+\tau_g)}{\Omega_\kappa}\right\}\right) \end{aligned} \quad (11)$$

can be rewritten as

$$\begin{aligned} & G_r(n, n+\tau) \\ & = \frac{1}{U^\lambda} \sum_{g=0}^{U^\lambda-1} E\{\kappa_\varsigma(r^{i_1}(n_g) - r^{i_2}(n_g+\tau_g)) \mathcal{J}(n_g, n_g+\tau_g)\} \\ & = \frac{1}{U^\lambda} \sum_{g=0}^{U^\lambda-1} \frac{\varsigma}{2\upsilon\Gamma(1/\varsigma)} E\left\{\frac{r^{i_1}(n_g)\, r^{i_2}(n_g+\tau_g)}{\Omega_\kappa}\right\}, \end{aligned} \tag{10}$$

where $\Omega_\kappa^{-1} = \exp\left(-\left|\frac{r^{i_1}(n_g) - \xi_g r^{i_2}(n_g+\tau_g) + |\vartheta|}{\upsilon}\right|^\varsigma\right)$. Assuming that the signal $s^{i_j}(n)$, the impulsive interference $I^{i_j}(n)$ and the Gaussian noise $w^{i_j}(n)$ are all uncorrelated, $G_r(n, n+\tau)$ can be further written as in (11) at the bottom of the page.

Let $G_s(n,n+\tau) = \frac{1}{U^\lambda}\sum_{g=0}^{U^\lambda-1}\left\{\frac{\tilde{s}^{i_1}(n_g)\tilde{s}^{i_2}(n_g+\tau_g)}{\Omega_\kappa}\right\}$, $G_I(n,n+\tau) = \frac{1}{U^\lambda}\sum_{g=0}^{U^\lambda-1}\left\{\frac{I^{i_1}(n_g)I^{i_2}(n_g+\tau_g)}{\Omega_\kappa}\right\}$ and $G_w(n,n+\tau) = \frac{1}{U^\lambda}\sum_{g=0}^{U^\lambda-1}\left\{\frac{w^{i_1}(n_g)w^{i_2}(n_g+\tau_g)}{\Omega_\kappa}\right\}$, $G_r(n, n+\tau)$ can be further expressed as

$$G_r(n,n+\tau) \approx A_\varsigma[G_s(n,n+\tau) + G_I(n,n+\tau) + G_w(n,n+\tau)]. \tag{12}$$

where $A_\varsigma = \varsigma/2\upsilon\Gamma(1/\varsigma)$.

In order to facilitate the analysis, for the condition of high signal-to-noise ratio, $G_r(n, n+\tau)$ can be approximated as

$$\begin{aligned} & G_r(n, n+\tau) \approx G_s(n, n+\tau) \\ & \approx \frac{A_\varsigma}{U^\lambda C_s} \sum_{g=0}^{U^\lambda-1} E\{\tilde{s}^{i_1}(n_g)\, \tilde{s}^{i_2}(n_g+\tau_g)\}, \end{aligned} \tag{13}$$

where $C_s^{-1} \approx \exp\left(-\left|\frac{I^{i_1}(n_g) - \xi_g I^{i_2}(n_g+\tau_g) + |\vartheta|}{\upsilon}\right|^\varsigma\right)$ is related to the amplitude of the impulsive interference for smaller characteristic exponent.

Based on the above discussion and the analysis in [18], the following observations can be made for different STBC-OFDM signals.

Lemma 1: For SM-OFDM signal, the generalized cross-correntropy is approximately equal to zero, i.e., $G_r(n, n+\tau) \approx 0$.

Proof: Considering that the signal $s^i(n)$, the impulsive interference $I^i(n)$ and the Gaussian noise $w^i(n)$ are uncorrelated, the Gaussian noise and the impulsive interference are assumed to be independent and identically distributed. From (1) and (6), we can obtain

$$E\left\{x_m^{f_1}(n_1)\, x_{m'}^{f_2}(n_2)\right\} = 0. \tag{14}$$

According to (13) and (14), $G_r(n, n+\tau)$ can be approximated as

$$G_r(n, n+\tau) \approx 0. \tag{15}$$

■

Lemma 2: The generalized cross-correntropy for AL-OFDM signal is nonzero only at $\tau = 1$, that is, $G_r^{\mathrm{AL}}(n, n+1)$ exhibits peaks.

Proof: For different moments at different antennas the symbols, $x_{2m+0}^{f_1}(n_1)$ and $x_{2m+1}^{f_2}(n_2)$ exhibit the following properties in (16) and (17) at the bottom of the page.

Using (16) and (17), $G_r^{\mathrm{AL}}(n, n+1)$ can be approximated as

$$G_r^{\mathrm{AL}}(n, n+1) \approx B_1 \sum_{\rho=-\infty}^{\infty} \sum_{l,l'=0}^{L_h-1} \eta_1(l, l')\, \delta(n - \rho_l), \tag{18}$$

where $B_1 = A_\varsigma C_{\sigma_s}^1 / C_s$, C_{σ_s} is associated with σ_s^2, $\eta_1(l, l')$ is a polynomial with respect to $h_{fi}(l)$ and ρ_l is a polynomial with parameters of l, N_z and ν. ■

Lemma 3: The generalized cross-correntropy for STBC3-OFDM signal is nonzero values at $\tau = 2$, that is, $G_r^{\mathrm{STBC3}}(n, n+2)$ exhibits nonzero magnitudes.

Proof: Based on the coding matrix in (3), $E\left\{x_{4m+u}^{f_1}(n_1)\, x_{4m'+u'}^{f_2}(n_2)\right\}$ can be expressed as

$$\begin{aligned} & E\left\{x_{4m+u}^{f_1}(n_1)\, x_{4m+u}^{f_2}(n_2)\right\} \\ & = \begin{cases} \sigma_s^2 \mathcal{M}(n_1, n_2, m, m) & \forall (f_1, f_2, u, u') \in \mathrm{T}_3 \\ -\sigma_s^2 \mathcal{M}(n_1, n_2, m, m) & \forall (f_1, f_2, u, u') \in \mathrm{T}_4 \\ 0 & otherwise, \end{cases} \end{aligned} \tag{19}$$

where $\mathcal{M}(n_1, n_2, m, m) = \delta(\mathrm{mod}(n_1+n_2, N_z))\, \delta(m - m')$, T_3 and T_4 represent the value set of variables (f_1, f_2, u, u').

From (13) and (19), we can obtain

$$G^{\mathrm{STBC3}}(n, n+2) \approx B_2 \sum_{\rho=-\infty}^{\infty} \sum_{l,l'=0}^{L_h-1} \eta_2(l, l')\, \delta(n - \rho_l), \tag{20}$$

$$\begin{aligned} E\left\{x_{2m+0}^{f_1}(n_1)\, x_{2m+1}^{f_2}(n_2)\right\} & = \frac{1}{N_z} \sum_{k,\tilde{k}}^{N_z-1} \left\{d_{2m+0}(k)\, d_{2m+0}^*\left(\tilde{k}\right)\right\} \exp\left(\frac{j2\pi\left(kn_1 + \tilde{k}n_2\right)}{N_z}\right) \\ & = \frac{\sigma_s^2}{N_z} \sum_{k}^{N_z-1} \exp\left(\frac{j2\pi k(n_1+n_2)}{N_z}\right) \\ & = \sigma_s^2 \delta(\mathrm{mod}(n_1+n_2, N_z)) \end{aligned} \tag{16}$$

$$\begin{aligned} E\left\{x_{2m+1}^{f_1}(n_1)\, x_{2m+0}^{f_2}(n_2)\right\} & = \frac{1}{N_z} \sum_{k,\tilde{k}}^{N_z-1} \left\{-d_{2m+1}(k)\, d_{2m+1}^*\left(\tilde{k}\right)\right\} \exp\left(\frac{j2\pi\left(kn_1 + \tilde{k}n_2\right)}{N_z}\right) \\ & = -\sigma_s^2 \delta(\mathrm{mod}(n_1+n_2, N_z)) \end{aligned} \tag{17}$$

where $B_2 = A_\varsigma C_{\sigma_s}^2 / C_s$, $\eta_2(l,l')$ is a polynomial with respect to $h_{fi}(l)$. ■

Lemma 4: The generalized cross-correntropy for STBC4-OFDM signal is nonzero when $\tau = 4$, that is, $G_r^{\mathrm{STBC4}}(n,n+4)$ exhibits discriminating peaks.

Proof: STBC4-OFDM According to the coding matrix in (4), $E\left\{x_{8m+u}^{f_1}(n_1)\, x_{8m'+u'}^{f_2}(n_2)\right\}$ can be written as

$$E\left\{x_{8m+u}^{f_1}(n_1)\, x_{8m+u}^{f_2}(n_2)\right\} = \begin{cases} \sigma_s^2 \mathcal{M}(n_1,n_2,m,m) & \forall (f_1,f_2,u,u') \in \mathrm{T}_5 \\ -\sigma_s^2 \mathcal{M}(n_1,n_2,m,m) & \forall (f_1,f_2,u,u') \in \mathrm{T}_6 \\ 0 & \mathit{otherwise.} \end{cases} \tag{21}$$

Based on (13) and (21), we can obtain

$$G^{\mathrm{STBC4}}(n,n+4) \approx B_3 \sum_{\rho=-\infty}^{\infty} \sum_{l,l'=0}^{L_h-1} \eta_3(l,l')\, \delta(n-\rho_l), \tag{22}$$

where $B_3 = A_\varsigma C_{\sigma_s}^3 / C_s$, $\eta_3(l,l')$ is a polynomial with respect to $h_{fi}(l)$. ■

Remark 1: Based on lemma 1- lemma 4, we note that the generalized cross-correntropy $G_r(n,n+\tau)$ exhibits significant differences for different STBC-OFDM signals at different values of τ. More specifically, $G_r(n,n+\tau)$ for SM-OFDM does not exhibit peaks at τ, and $G_r(n,n+\tau)$ exhibits peaks for AL-OFDM, STBC3-OFDM and STBC4-OFDM when $\tau=1$, $\tau=2$ and $\tau=4$. Furthermore, STBC4-OFDM can be distinguished from STBC3-OFDM, AL-OFDM and SM-OFDM by utilizing $G_r(n,n+\tau)$ at $\tau=4$; STBC3-OFDM can be discriminated from AL-OFDM and SM-OFDM by exploiting $G_r(n,n+\tau)$ at $\tau=2$; SM-OFDM can be identified from AL-OFDM by using $G_r(n,n+\tau)$ at $\tau=1$.

In the following, we will develop a novel decision tree classification scheme for STBC-OFDM signals. First, the feature matrix of the generalized cross-correntropy is employed to construct the discriminating matrix for different STBC-OFDM signals. Using the discriminating matrix, the test statistic and detection threshold will be constructed in a sequential binary hypothesis test. Finally, a decision tree identification algorithm will be developed to identify the STBC-OFDM signals.

B. STBC-OFDM Identification Scheme

In practice, it is usually not possible to obtain the generalized cross-correntropy. Hence, it is generally estimated as

$$\begin{aligned} &\hat{G}_r^{(i_1,i_2)}(n,n+\tau) \\ &= \frac{1}{N_b}\sum_{k=0}^{N_b-1}\left\{\kappa_\varsigma\left(r^{i_1}(n_k) - r^{i_2}(n_k+\tau_k)\right)\mathcal{J}(n_k,n_k+\tau_k)\right\} \\ &= \frac{1}{N_b}\sum_{k=0}^{N_b-1}\left\{r^{i_1}(n_k)\, r^{i_2}(n_k+\tau_k)\right. \\ &\quad \times \exp\left(-\left|\frac{r^{i_1}(n_k) - \xi_k r^{i_2}(n_k+\tau_k) + |\vartheta|}{\upsilon}\right|^{\varsigma}\right)\Bigg\} \\ &\approx \tilde{G}_s(n,n+\tau) + \tilde{\varepsilon}_G(n,n+\tau), \end{aligned} \tag{23}$$

where $\mathcal{J}(n_k,n_k+\tau_k) = r^{i_1}(n_k)\, r^{i_2}(n_k+\tau_k)$, $n_k = n + k(N_z+\nu)$, $n_k+\tau_k = n+(k+\tau)(N_z+\nu)$, and $\tilde{\varepsilon}_G(n,n+\tau)$ is the estimation error.

Without loss of generality, we first use SM and AL as illustrative examples. When $N_b \to \infty$, the generalized cross-correntropy estimator $\hat{G}_r^{(i_1,i_2)}(n,n+\tau)$ approximately approaches zero for SM, and it exhibits the peak value for AL. Based on this, the following hypothesis testing is formulated to differentiate the AL-OFDM and SM-OFDM signals as

$$\begin{cases} \mathcal{H}_0: \hat{G}_r^{(i_1,i_2)}(n,n+\tau) = \tilde{\varepsilon}_G(n,n+\tau) \\ \mathcal{H}_1: \hat{G}_r^{(i_1,i_2)}(n,n+\tau) = \tilde{G}_{\mathrm{AL}}(n,n+\tau) + \tilde{\varepsilon}_G(n,n+\tau), \end{cases} \tag{24}$$

where $\mathcal{H}_0$ denotes the hypothesis that SM-OFDM is ture and $\mathcal{H}_1$ represents that AL-OFDM is ture.

For multiple receive antennas, we denote a set of receive antenna pairs as

$$\Upsilon = \{(i_1,i_2) : i_1 \neq i_2, 1 \leq i_1 \leq M_r, 1 \leq i_2 \leq M_r\}. \tag{25}$$

Based on (23), we obtain the generalized cross-correntropy feature matrix for the antenna index set Υ as

$$\hat{\mathbf{G}}_{\mathbf{r}}^{\tau} = \left[\left|\hat{G}_r^{(1,2)}(n,n+\tau)\right| \ \cdots \ \left|\hat{G}_r^{(M_r-1,M_r)}(n,n+\tau)\right|\right]^{\mathrm{T}}, \tag{26}$$

where $n \in [0,P_n]$ $P_n > N_z/2+\nu$ and $\hat{G}_r^{(i_1,i_2)}(n,n+\tau)$ denotes the generalized cross-correntropy of the signals from different receiving antennas.

According to (15) and (26), the feature matrix $\hat{\mathbf{G}}_{\mathrm{SM}}^{\tau=1}$ of SM-OFDM can be expressed as

$$\hat{\mathbf{G}}_{\mathrm{SM}}^{\tau=1} = \left[\tilde{\varepsilon}_G^{(1,2)}(n,n+1) \ \cdots \ \tilde{\varepsilon}_G^{(M_r-1,M_r)}(n,n+1)\right]^{\mathrm{T}}. \tag{27}$$

Similarly, the feature matrix $\hat{\mathbf{G}}_{\mathrm{AL}}^{\tau=1}$ can be given as (28) at the bottom of the page.

We recall that $\hat{G}_{\mathrm{AL}}^{(i_1,i_2)}(n,n+1)$ exhibits the peaks when $n=\rho_l$, and $\hat{G}_{\mathrm{SM}}^{(i_1,i_2)}(n,n+1)$ does not exhibit peaks. From the discussion, we extract the elements of the peak position in the feature matrix to construct the discriminating matrix as

$$\mathbf{V}_{\mathbf{G}}^{\tau=1} = \left[\left|\hat{G}_r^{(1,2)}(v_1,v_1+1)\right| \cdots \left|\hat{G}_r^{(M_r-1,M_r)}(v_{L_e},v_{L_e}+1)\right|\right]^{\mathrm{T}}, \tag{29}$$

$$\hat{\mathbf{G}}_{\mathrm{AL}}^{\tau=1} = \left[\tilde{G}_{\mathrm{AL}}^{(1,2)}(n,n+1) + \tilde{\varepsilon}_G^{(1,2)}(n,n+1) \ \cdots \ \tilde{G}_{\mathrm{AL}}^{(M_r-1,M_r)}(n,n+1) + \tilde{\varepsilon}_G^{(M_r-1,M_r)}(n,n+1)\right]^{\mathrm{T}} \tag{28}$$

where v_e represents the e-th peak position in $\left|\tilde{G}_{\mathrm{AL}}^{(i_1,i_2)}(n,n+1)\right|$. To reduce the error, we extend the peak position by discriminating all Δ values around v_e, i.e. $\tilde{v}_l \in [v_e-\Delta, v_e+\Delta]$. Hence, the discriminating matrix $\tilde{\mathbf{V}}_{\mathbf{G}}^{\tau=1}$ can be further expressed as

$$\tilde{\mathbf{V}}_{\mathbf{G}}^{\tau=1}=\left[\left|\hat{G}_r^{(1,2)}(\tilde{v}_1,\tilde{v}_1+1)\right|\cdots\left|\hat{G}_r^{(M_r-1,M_r)}(\tilde{v}_{L_e},\tilde{v}_{L_e}+1)\right|\right]^{\mathrm{T}}, \quad (30)$$

where the discriminating matrix $\tilde{\mathbf{V}}_{\mathbf{G}}^{\tau=1}$ for $\hat{\mathbf{G}}_{\mathrm{AL}}^{\tau=1}$ contains large non-zero peaks, while the elements of $\tilde{\mathbf{V}}_{\mathbf{G}}^{\tau=1}$ for $\hat{\mathbf{G}}_{\mathrm{SM}}^{\tau=1}$ remain as error terms. Thus, we can exploit the discriminating matrix $\tilde{\mathbf{V}}_{\mathbf{G}}^{\tau=1}$ to obtain the test statistic $T_{\hat{\mathbf{G}}_{\mathbf{r}}^{\tau=1}}$ as

$$T_{\hat{\mathbf{G}}_{\mathbf{r}}^{\tau=1}}=\frac{1}{L_{\tilde{\mathbf{V}}}^{\tau=1}I_{\tilde{\mathbf{V}}}^{\tau=1}}\left\|\tilde{\mathbf{V}}_{\mathbf{G}}^{\tau=1}\right\|_{l_1}, \quad (31)$$

where $L_{\tilde{\mathbf{V}}}^{\tau=1}$ and $I_{\tilde{\mathbf{V}}}^{\tau=1}$ are the numbers of rows and columns of matrix $\tilde{\mathbf{V}}_{\mathbf{G}}^{\tau=1}$, respectively, and $\|\mathbf{U}\|_{l_1}$ denotes the sum of the absolute values of elements in matrix $\mathbf{U}$.

According to the test statistic $T_{\hat{\mathbf{G}}_{\mathbf{r}}^{\tau=1}}$, we formulate the decision criterion as

$$\begin{cases}\mathcal{H}_0: T_{\hat{\mathbf{G}}_{\mathbf{r}}^{\tau=1}} \le \psi_{\hat{\mathbf{G}}_{\mathbf{r}}^{\tau=1}}\\ \mathcal{H}_1: T_{\hat{\mathbf{G}}_{\mathbf{r}}^{\tau=1}} > \psi_{\hat{\mathbf{G}}_{\mathbf{r}}^{\tau=1}},\end{cases} \quad (32)$$

where $\psi_{\hat{\mathbf{U}}_{\mathbf{r}}^{\tau=1}}$ represents the decision threshold. Under $\mathcal{H}_0$, the test statistic $T_{\hat{\mathbf{G}}_{\mathbf{r}}^{\tau=1}}$ is not greater than the decision threshold $\psi_{\hat{\mathbf{G}}_{\mathbf{r}}^{\tau=1}}$, i.e., $\hat{\mathbf{G}}_{\mathbf{r}}^{\tau=1}$ does not exhibit peaks. Under $\mathcal{H}_1$ hypothesis, there is least one peak in $\hat{\mathbf{G}}_{\mathbf{r}}^{\tau=1}$. Based on the central limit theorem, $|\tilde{\varepsilon}_G(n,n+1)|$ approximately follows a Gaussian distribution for sufficiently large N_b. As a result, we can set the detection threshold as

$$\psi_{\hat{\mathbf{G}}_{\mathbf{r}}^{\tau=1}}=\mu_{T_{\mathbf{G}}|\mathcal{H}_0}+t_\psi\sigma_{T_{\mathbf{G}}|\mathcal{H}_0}, \quad (33)$$

where $\mu_{T_{\mathbf{G}}|\mathcal{H}_0}$ and $\sigma^2_{T_{\mathbf{G}}|\mathcal{H}_0}$ are the moment and variance of $T_{\hat{\mathbf{U}}_{\mathbf{r}}^{\tau=1}}$ under $\mathcal{H}_0$, respectively.

Then, $T_{\hat{\mathbf{G}}_{\mathbf{r}}^{\tau=1}}$ under $\mathcal{H}_0$ is used to estimate $\mu_{T_{\mathbf{G}}|\mathcal{H}_0}$ and $\sigma^2_{T_{\mathbf{G}}|\mathcal{H}_0}$.

Based on (27) and (28), the elements of $\hat{\mathbf{G}}_{\mathrm{SM}}^{\tau=1}$ can be expressed as

$$\hat{G}_{\mathrm{SM}}^{(i_1,i_2)}(n,n+1)=\tilde{\varepsilon}_G^{(i_1,i_2)}(n,n+1), \quad (34)$$

and the elements of $\hat{\mathbf{U}}_{\mathrm{AL}}^{\tau=1}$ can be written as

$$\hat{G}_{\mathrm{AL}}^{(i_1,i_2)}(n,n+1)=\tilde{G}_{\mathrm{AL}}^{(i_1,i_2)}(n,n+1)+\tilde{\varepsilon}_G^{(i_1,i_2)}(n,n+1). \quad (35)$$

By comparing (34) and (35), we can see that the main difference between $\hat{G}_{\mathrm{AL}}^{(i_1,i_2)}(n,n+1)$ and $\hat{G}_{\mathrm{SM}}^{(i_1,i_2)}(n,n+1)$ is attributed to $\tilde{G}_{\mathrm{AL}}^{(i_1,i_2)}(n,n+1)$. If the elements of the discriminating matrix $\tilde{\mathbf{V}}_{\mathbf{G}}^{\tau=1}$ are removed from the feature matrix $\hat{\mathbf{G}}_{\mathbf{r}}^{\tau=1}$, the error matrix $\tilde{\mathbf{E}}_{\mathbf{G}}^{\tau=1}$ is obtained, which consists of the error term $\tilde{\varepsilon}_U^{(i_1,i_2)}(n,n+1)$ as

$$\tilde{\mathbf{E}}_{\mathbf{G}}^{\tau=\mathbf{1}}=\hat{\mathbf{G}}_{\mathbf{r}}^{\tau=1}\copyright\tilde{\mathbf{V}}_{\mathbf{G}}^{\tau=1}, \quad (36)$$

where $\mathbf{A}\copyright\mathbf{B}$ denotes the removal of elements of matrix $\mathbf{B}$ from matrix $\mathbf{A}$.

As mentioned previously, it is clear that the elements of $\tilde{\mathbf{V}}_{\mathbf{G}}^{\tau=1}$ for $\hat{\mathbf{U}}_{\mathrm{SM}}^{\tau=1}$ are error terms, and the elements of the error matrix $\tilde{\mathbf{E}}_{\mathbf{G}}^{\tau=\mathbf{1}}$ are similarly error terms. Therefore, the moment of $T_{\hat{\mathbf{U}}_{\mathbf{r}}^{\tau=1}}$ under $\mathcal{H}_0$ can be approximated as

$$\hat{\mu}_{T_{\mathbf{G}}|\mathcal{H}_0}=\frac{1}{L_{\tilde{\mathbf{E}}}^{\tau=1}I_{\tilde{\mathbf{E}}}^{\tau=1}}\left\|\tilde{\mathbf{E}}_{\mathbf{G}}^{\tau=\mathbf{1}}\right\|_{l_1}, \quad (37)$$

where $L_{\tilde{\mathbf{E}}}^{\tau=1}$ and $I_{\tilde{\mathbf{E}}}^{\tau=1}$ denote the number of rows and columns of $\tilde{\mathbf{E}}_{\mathbf{G}}^{\tau=\mathbf{1}}$, respectively. $\|\mathbf{E}\|_{l_1}$ represents the sum of the absolute values of the elements in $\mathbf{E}$. Under $\mathcal{H}_0$, the variance of $T_{\hat{\mathbf{G}}_{\mathbf{r}}^{\tau=1}}$ can be approximated as

$$\hat{\sigma}^2_{T_{\mathbf{G}}|\mathcal{H}_0}=\frac{1}{L_{\tilde{\mathbf{E}}}^{\tau=1}I_{\tilde{\mathbf{E}}}^{\tau=1}}\left(\frac{1}{L_{\tilde{\mathbf{E}}}^{\tau=1}I_{\tilde{\mathbf{E}}}^{\tau=1}}\left\|\tilde{\mathbf{E}}_{\mathbf{G}}^{\tau=1}\right\|_{l_2}^2-\hat{\mu}^2_{T_{\mathbf{G}}|\mathcal{H}_0}\right), \quad (38)$$

where $\|\mathbf{E}\|_{l_2}^2$ is the sum of the squares of the absolute values of the elements in $\mathbf{E}$.

Using this discriminating matrix, we extend the binary hypothesis test to develop a decision tree scheme based on the generalized cross-correntropy for identifying the $\mathrm{STBC} \in \{\mathrm{STBC4}, \mathrm{STBC3}, \mathrm{AL}, \mathrm{SM}\}$. The structure of the decision tree identification algorithm is shown in Fig. 2. As shown in Fig. 2, the STBC4 is distinguished from $\{\mathrm{STBC3}, \mathrm{AL}, \mathrm{SM}\}$ at the top-level node of the decision tree. The generalized cross-correntropy feature matrix $\hat{\mathbf{G}}_{\mathbf{r}}^{\tau=4}$ for $\tau=4$ is calculated to extract the discriminating matrix $\tilde{\mathbf{V}}_{\mathbf{G}}^{\tau=4}$ and the error matrix $\tilde{\mathbf{E}}_{\mathbf{G}}^{\tau=\mathbf{4}}$, which in turn constructs the test statistic $T_{\hat{\mathbf{G}}_{\mathbf{r}}^{\tau=4}}$ and detection threshold $\psi_{\hat{\mathbf{G}}_{\mathbf{r}}^{\tau=4}}$. Correspondingly, the generalized cross-correntropy feature matrix $\hat{\mathbf{G}}_{\mathbf{r}}^{\tau=4}$ can be expressed as

$$\hat{\mathbf{G}}_{\mathbf{r}}^{\tau=4}=\left[\left|\hat{G}_r^{(1,2)}(n,n+4)\right|,\cdots,\left|\hat{G}_r^{(M_r-1,M_r)}(n,n+4)\right|\right]^{\mathrm{T}}. \quad (39)$$

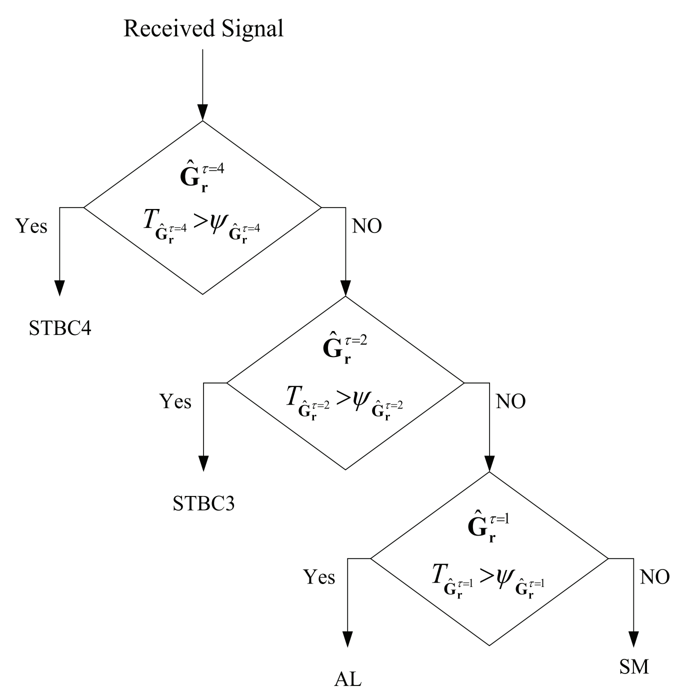

Fig. 2. Decision tree based on the generalized cross-correntropy function for the identification of STBC-OFDM signals.

Using the feature matrix $\hat{\mathbf{G}}_{\mathbf{r}}^{\tau=4}$, the discriminating matrix $\tilde{\mathbf{V}}_{\mathbf{G}}^{\tau=4}$ can be constructed as

$$\tilde{\mathbf{V}}_{\mathbf{G}}^{\tau=4}=\left[\left|\hat{G}_r^{(1,2)}(\tilde{v}_1,\tilde{v}_1+4)\right|,\cdots,\left|\hat{G}_r^{(M_r-1,M_r)}(\tilde{v}_{L_e},\tilde{v}_{L_e}+4)\right|\right]^{\mathrm{T}}. \quad (40)$$

According to (40), the detection statistic $T_{\hat{\mathbf{G}}_{\mathbf{r}}^{\tau=4}}$ at the top-level node is expressed as

$$T_{\hat{\mathbf{G}}_{\mathbf{r}}^{\tau=4}}=\frac{1}{L_{\tilde{\mathbf{V}}}^{\tau=4}I_{\tilde{\mathbf{V}}}^{\tau=4}}\left\|\tilde{\mathbf{V}}_{\mathbf{G}}^{\tau=4}\right\|_{l_1}. \quad (41)$$

By exploiting the feature matrix $\hat{\mathbf{G}}_{\mathbf{r}}^{\tau=4}$ and the discriminating matrix $\tilde{\mathbf{V}}_{\mathbf{G}}^{\tau=4}$, the error matrix can be obtained as

$$\tilde{\mathbf{E}}_{\mathbf{G}}^{\tau=4}=\hat{\mathbf{U}}_{\mathbf{r}}^{\tau=4}\circledcirc\tilde{\mathbf{V}}_{\mathbf{G}}^{\tau=4}. \quad (42)$$

Now, using the error matrix $\tilde{\mathbf{E}}_{\mathbf{G}}^{\tau=4}$, the moment $\hat{\mu}_{T_{\mathbf{G}}^{C_1}|\mathcal{H}_0}$ and variance $\hat{\sigma}^2_{T_{\mathbf{G}}^{C_1}|\mathcal{H}_0}$ can be expressed as

$$\hat{\mu}_{T_{\mathbf{G}}^{C_1}|\mathcal{H}_0}=\frac{1}{L_{\tilde{\mathbf{E}}}^{\tau=4}I_{\tilde{\mathbf{E}}}^{\tau=4}}\left\|\tilde{\mathbf{E}}_{\mathbf{G}}^{\tau=4}\right\|_{l_1}, \quad (43)$$

$$\hat{\sigma}^2_{T_{\mathbf{G}}^{C_1}|\mathcal{H}_0}=\frac{1}{L_{\tilde{\mathbf{E}}}^{\tau=4}I_{\tilde{\mathbf{E}}}^{\tau=4}}\left(\frac{1}{L_{\tilde{\mathbf{E}}}^{\tau=4}I_{\tilde{\mathbf{E}}}^{\tau=4}}\left\|\tilde{\mathbf{E}}_{\mathbf{G}}^{\tau=4}\right\|_{l_2}^2-\hat{\mu}^2_{T_{\mathbf{G}}^{C_1}|\mathcal{H}_0}\right). \quad (44)$$

Using (43) and (44), the detection threshold $\psi_{\hat{\mathbf{G}}_{\mathbf{r}}^{\tau=4}}$ is obtained as

$$\psi_{\hat{\mathbf{G}}_{\mathbf{r}}^{\tau=4}}=\hat{\mu}_{T_{\mathbf{G}}^{C_1}|\mathcal{H}_0}+t_\psi\hat{\sigma}_{T_{\mathbf{G}}^{C_1}|\mathcal{H}_0}. \quad (45)$$

If $T_{\hat{\mathbf{G}}_{\mathbf{r}}^{\tau=4}}>\psi_{\hat{\mathbf{G}}_{\mathbf{r}}^{\tau=4}}$, the received signal is identified as STBC4, otherwise go to the middle level node of the decision tree.

Similarly, the generalized cross-correntropy feature matrix $\hat{\mathbf{G}}_{\mathbf{r}}^{\tau=2}$ is exploited to discriminate STBC3 from $\{\mathrm{AL},\mathrm{SM}\}$ at the middle level node. The detection statistic $T_{\hat{\mathbf{G}}_{\mathbf{r}}^{\tau=2}}$ at the middle level node is expressed as

$$T_{\hat{\mathbf{G}}_{\mathbf{r}}^{\tau=2}}=\frac{1}{L_{\tilde{\mathbf{V}}}^{\tau=2}I_{\tilde{\mathbf{V}}}^{\tau=2}}\left\|\tilde{\mathbf{V}}_{\mathbf{G}}^{\tau=2}\right\|_{l_1}, \quad (46)$$

with $\tilde{\mathbf{V}}_{\mathbf{U}}^{\tau=2}$ given as

$$\tilde{\mathbf{V}}_{\mathbf{G}}^{\tau=2}=\left[\left|\hat{G}_r^{(1,2)}(\tilde{v}_1,\tilde{v}_1+2)\right|,\cdots,\left|\hat{G}_r^{(M_r-1,M_r)}(\tilde{v}_{L_e},\tilde{v}_{L_e}+2)\right|\right]^{\mathrm{T}}, \quad (47)$$

where the feature matrix$\hat{\mathbf{G}}_{\mathbf{r}}^{\tau=2}$ can be expressed as

$$\hat{\mathbf{G}}_{\mathbf{r}}^{\tau=2}=\left[\left|\hat{G}_r^{(1,2)}(n,n+2)\right|\cdots\left|\hat{G}_r^{(M_r-1,M_r)}(n,n+2)\right|\right]^{\mathrm{T}}. \quad (48)$$

Similar to $\psi_{\hat{\mathbf{G}}_{\mathbf{r}}^{\tau=4}}$, the detection threshold $\psi_{\hat{\mathbf{G}}_{\mathbf{r}}^{\tau=2}}$ can be obtained as

$$\psi_{\hat{\mathbf{G}}_{\mathbf{r}}^{\tau=2}}=\hat{\mu}_{T_{\mathbf{G}}^{C_2}|\mathcal{H}_0}+t_\psi\hat{\sigma}_{T_{\mathbf{G}}^{C_2}|\mathcal{H}_0}, \quad (49)$$

where $\hat{\mu}_{T_{\mathbf{G}}^{C_2}|\mathcal{H}_0}$ and $\hat{\sigma}^2_{T_{\mathbf{G}}^{C_2}|\mathcal{H}_0}$ can be expressed as

$$\hat{\mu}_{T_{\mathbf{G}}^{C_2}|\mathcal{H}_0}=\frac{1}{L_{\tilde{\mathbf{E}}}^{\tau=2}I_{\tilde{\mathbf{E}}}^{\tau=2}}\left\|\tilde{\mathbf{E}}_{\mathbf{G}}^{\tau=2}\right\|_{l_1}, \quad (50)$$

$$\hat{\sigma}^2_{T_{\mathbf{G}}^{C_2}|\mathcal{H}_0}=\frac{1}{L_{\tilde{\mathbf{E}}}^{\tau=2}I_{\tilde{\mathbf{E}}}^{\tau=2}}\left(\frac{1}{L_{\tilde{\mathbf{E}}}^{\tau=2}I_{\tilde{\mathbf{E}}}^{\tau=2}}\left\|\tilde{\mathbf{E}}_{\mathbf{G}}^{\tau=2}\right\|_{l_2}^2-\hat{\mu}^2_{T_{\mathbf{G}}^{C_2}|\mathcal{H}_0}\right), \quad (51)$$

with

$$\tilde{\mathbf{E}}_{\mathbf{G}}^{\tau=2}=\hat{\mathbf{G}}_{\mathbf{r}}^{\tau=2}\circledcirc\tilde{\mathbf{V}}_{\mathbf{G}}^{\tau=2}. \quad (52)$$

If $T_{\hat{\mathbf{G}}_{\mathbf{r}}^{\tau=2}}>\psi_{\hat{\mathbf{G}}_{\mathbf{r}}^{\tau=2}}$, the received signal is determined as STBC3; otherwise, at the bottom level node of the decision tree, AL and SM are identified by using the test statistic $T_{\hat{\mathbf{G}}_{\mathbf{r}}^{\tau=1}}$ in (31) and the detection threshold $\psi_{\hat{\mathbf{G}}_{\mathbf{r}}^{\tau=1}}$ in (33).

The procedure of STBC-OFDM identification algorithm based on the generalized cross-correntropy function is summarized in Algorithm 1.

Algorithm 1: Identification of STBC-OFDM based on generalized cross-correntropy function.

Input : The observed signal $\mathbf{r}(n)$.
Output: STBC

1 Initialize parameters $\tau=4$.
2 Calculate the generalized cross-correntropy feature matrix $\hat{\mathbf{G}}_{\mathbf{r}}^{\tau=4}$.
3 Extract the discriminating matrix $\tilde{\mathbf{V}}_{\mathbf{G}}^{\tau=4}$ and the error matrix $\tilde{\mathbf{E}}_{\mathbf{G}}^{\tau=\mathbf{4}}$ by utilizing $\hat{\mathbf{G}}_{\mathbf{r}}^{\tau=4}$.
4 Construct the test statistic $T_{\hat{\mathbf{G}}_{\mathbf{r}}^{\tau=4}}$ and detection threshold $\psi_{\hat{\mathbf{G}}_{\mathbf{r}}^{\tau=4}}$ by using $\tilde{\mathbf{V}}_{\mathbf{G}}^{\tau=4}$ and $\tilde{\mathbf{E}}_{\mathbf{G}}^{\tau=\mathbf{4}}$.
5 **if** $T_{\hat{\mathbf{G}}_{\mathbf{r}}^{\tau=4}}>\psi_{\hat{\mathbf{G}}_{\mathbf{r}}^{\tau=4}}$ **then**
6 the received signal is identified as STBC4 .
7 **else**
8 go to step 9.
9 Set parameters $\tau=2$ and calculate $\hat{\mathbf{G}}_{\mathbf{r}}^{\tau=2}$, $\tilde{\mathbf{V}}_{\mathbf{G}}^{\tau=2}$, $\tilde{\mathbf{E}}_{\mathbf{G}}^{\tau=\mathbf{2}}$, $T_{\hat{\mathbf{G}}_{\mathbf{r}}^{\tau=2}}$ and $\psi_{\hat{\mathbf{G}}_{\mathbf{r}}^{\tau=2}}$.
10 **if** $T_{\hat{\mathbf{G}}_{\mathbf{r}}^{\tau=2}}>\psi_{\hat{\mathbf{G}}_{\mathbf{r}}^{\tau=2}}$ **then**
11 the received signal is identified as STBC3.
12 **else**
13 go to step 14.
14 Set parameters $\tau=1$ and calculate $\hat{\mathbf{G}}_{\mathbf{r}}^{\tau=1}$, $\tilde{\mathbf{V}}_{\mathbf{G}}^{\tau=1}$, $\tilde{\mathbf{E}}_{\mathbf{G}}^{\tau=\mathbf{1}}$, $T_{\hat{\mathbf{G}}_{\mathbf{r}}^{\tau=1}}$ and $\psi_{\hat{\mathbf{G}}_{\mathbf{r}}^{\tau=1}}$.
15 **if** $T_{\hat{\mathbf{G}}_{\mathbf{r}}^{\tau=1}}>\psi_{\hat{\mathbf{G}}_{\mathbf{r}}^{\tau=1}}$ **then**
16 the received signal is identified as AL.
17 **else**
18 the received signal is SM.

IV. Simulation Results and Discussion

In this section, we will show the identification performance of the proposed algorithm using Monte Carlo simulation. We consider a MIMO-OFDM wireless communication system that employs STBC architecture. Unless otherwise mentioned, we consider an OFDM system with quadrature phase shift keying (QPSK). The number of sub-carriers is $N_z=64$, the cyclic prefix length is $\nu=N_z/4$. The number of observed blocks is $N_b=2000$ and the number of receive antennas is $M_r=4$. The width parameter and the shape parameter are set as $\upsilon=5$ and $\varsigma=0.3$. The Monte Carlo method is used to set the parameter t_ψ. The received signal was affected by Gaussian noise and symmetric alpha stable interference. The signal-to-interference ratio SIR is defined as $\mathrm{SIR}=E\left[\|\mathbf{r}(n)-\mathbf{I}(n)-\mathbf{w}(n)\|_{\mathrm{F}}^2\right]\Big/(M_r\gamma_\alpha)$, with γ_α being the dispersion coefficient of the symmetric alpha stable interference. Furthermore, the channel is assumed to be a frequency-selective Rayleigh fading channel consisting of

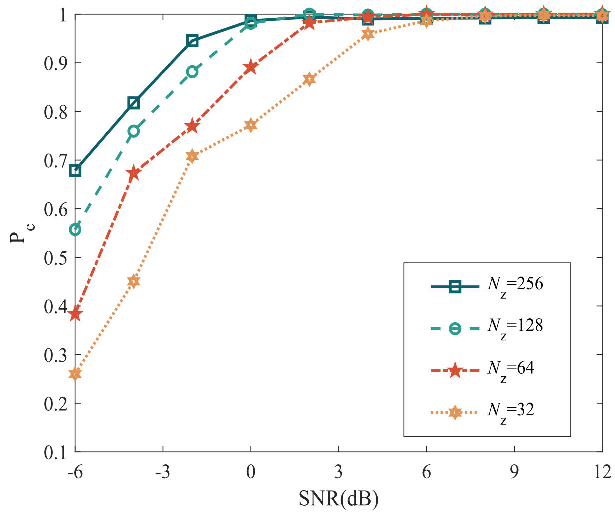

Fig. 3. Average probability of correct identification versus SNR for different numbers of OFDM subcarriers.

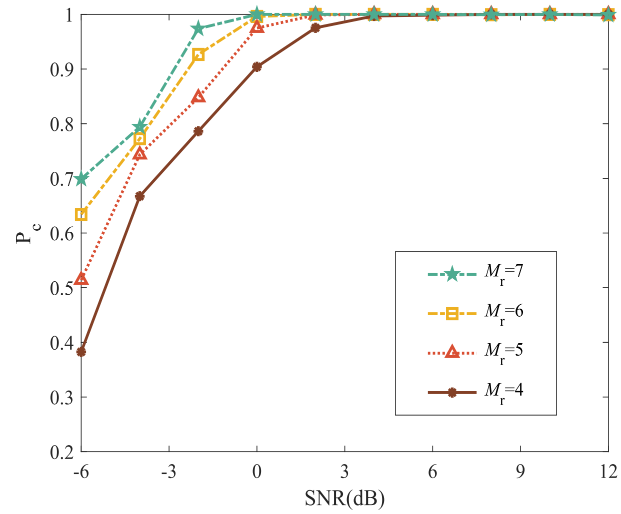

Fig. 4. Average probability of correct identification versus SNR for different numbers of receive antennas.

$L_h = 4$ statistically independent taps. For the performance of STBC-OFDM identification, the average probability of correct identification $\mathrm{P_c}$ is used as a performance measure, which is defined as

$$\mathrm{P_c} = \frac{1}{\mathrm{L}_\lambda} \sum \mathrm{P_r}\left(\hat{\mathrm{C}}_\mathrm{T} \,|\mathrm{C}_\mathrm{T}\right), \tag{53}$$

where $C_T \in \lambda$ and $\lambda = \{\mathrm{STBC4}, \mathrm{STBC3}, \mathrm{AL}, \mathrm{SM}\}$, L_λ denotes the number of elements of λ.

First, the influence of the number of OFDM subcarriers N_z on the identification performance of the proposed algorithm is analyzed. In Fig. 3, the average probability of correct identification $\mathrm{P_c}$ of STBC-OFDM signals is presented versus SNR for $N_z = 64, 128, 256$ in symmetric alpha stable interference. In the simulation, the cyclic prefix length of OFDM is $\nu = N_z/4$, $\mathrm{SIR} = 18\mathrm{dB}$, and the characteristic exponent is $\alpha = 1.8$. It is evident from Fig. 3 that the identification performance of the proposed algorithm improves significantly as the number of OFDM subcarriers N_z increases. For example, for $\mathrm{SNR} = 0\mathrm{dB}$, the average probability of correct detection is close to 0.98 with $N_z = 256$, and just 0.78 with $N_z = 64$. That is mainly because the generalized cross-correntropy features become much more significant when the number of OFDM subcarriers N_z increases, which facilitates the identification of different space-time coding types.

The effect of the number of receive antennas M_r on the identification performance of the proposed algorithm is then investigated. Fig. 4 shows the average probability of correct identification $\mathrm{P_c}$ of STBC-OFDM signals for different $M_r = 4$, $M_r = 5$, $M_r = 6$ and $M_r = 7$. The results in Fig. 4 show that the identification performance of the proposed algorithm based on the generalized cross-correntropy significantly improves by increasing M_r. For instance, the average probability of correct identification $\mathrm{P_c}$ is close to 0.97 with $M_r = 7$, and just 0.78 with $M_r = 4$, when $\mathrm{SNR} = -2\mathrm{dB}$ and $\mathrm{SIR} = 18\mathrm{dB}$. This is because the peak values in the discriminating matrix $\tilde{\mathbf{V}}_{\mathbf{G}}^{\tau}$ are significantly enhanced with increasing M_r, which make increasingly different the test statistic $T_{\hat{\mathbf{G}}_\mathrm{r}^\tau}$ and the detection

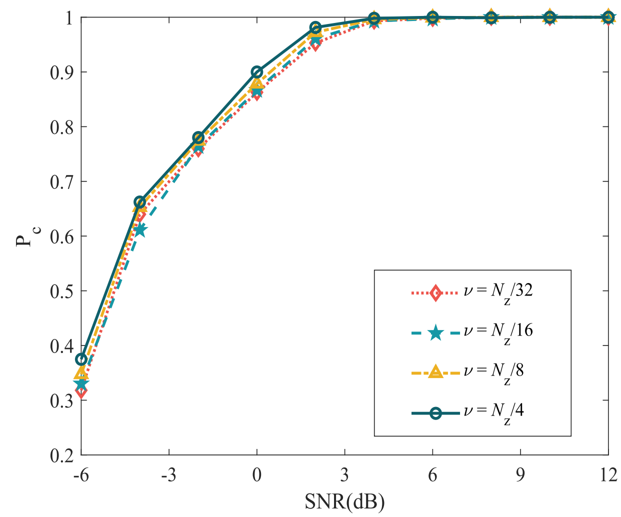

Fig. 5. Average probability of correct identification versus SNR for different cyclic prefix length.

threshold $\psi_{\hat{\mathbf{G}}_\mathrm{r}^\tau}$.

Fig. 5 illustrates the average probability of correct identification of the proposed algorithm is influenced by the different cyclic prefix length ν ($\nu = N_z/4$, $N_z/8$, $N_z/16$, $N_z/32$). From Fig. 5, it is observed that by increasing the cyclic prefix length ν, the performance slightly improves. For example, the average probability of correct identification $\mathrm{P_c}$ tends to 0.9 with $\nu = N_z/4$, and just 0.88 with $\nu = N_z/8$, when $\mathrm{SNR} = 0\mathrm{dB}$ and $\mathrm{SIR} = 18\mathrm{dB}$. This can be explained by the fact that the peak values in the discriminating matrix $\tilde{\mathbf{V}}_{\mathbf{G}}^{\tau}$ slightly increase with ν.

The effect of modulation on the proposed algorithm is shown in Fig. 6. From Fig. 6, when $\mathrm{SNR} = 0\mathrm{dB}$, the average probability of correct identification of the proposed algorithm approaches 0.9 for four modulation types with $\nu = N_z/4$, $\mathrm{SIR} = 18\mathrm{dB}$ and $\alpha = 1.8$. One can see that the performance of the proposed algorithm based on the generalized cross-

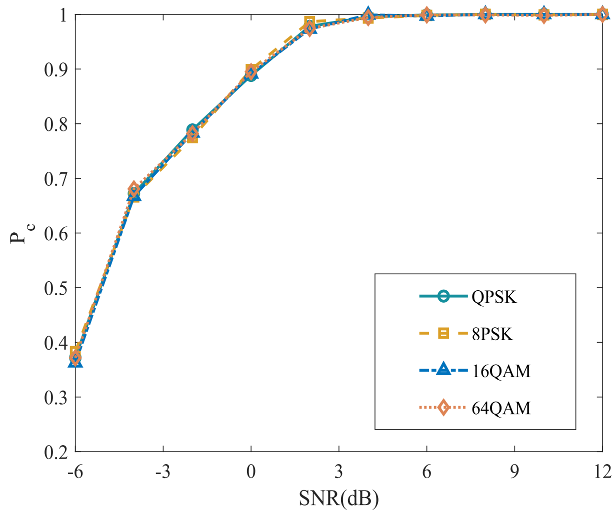

Fig. 6. The effect of the modulation type on the average probability of correct identification versus SNR.

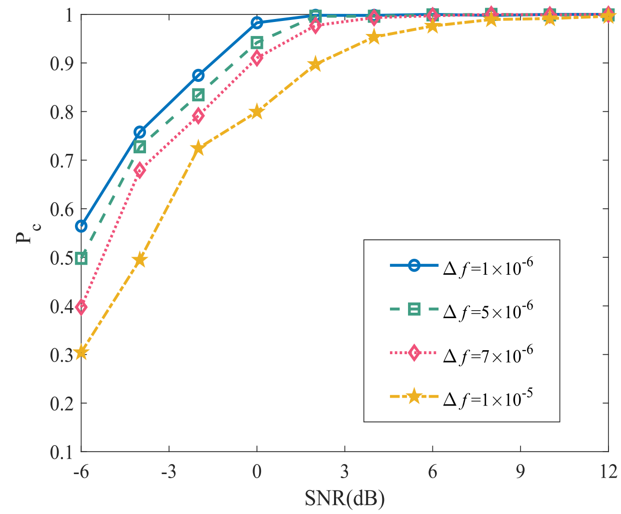

Fig. 8. The effect of the frequency offset on the average probability of correct identification versus SNR.

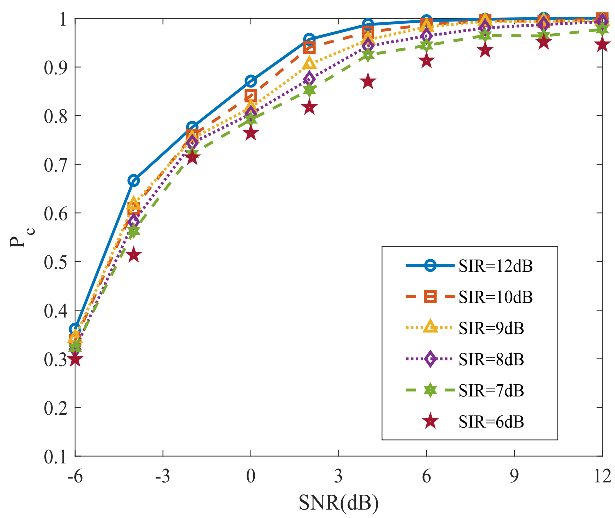

Fig. 7. The effect of the signal-to-interference ratio on the average probability of correct identification versus SNR.

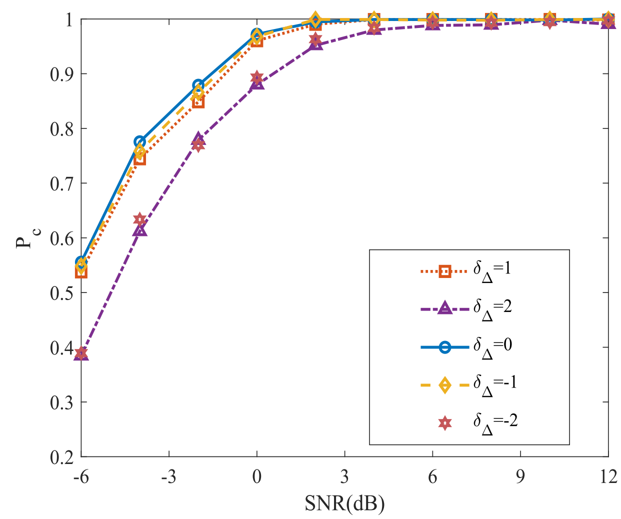

Fig. 9. The influence of the sample timing offset on the average probability of correct identification.

correntropy is not affected by the modulation type. The reason is that the discriminating matrix $\tilde{\mathbf{V}}_{\mathbf{G}}^{\tau}$ and the error matrix $\tilde{\mathbf{E}}_{\mathbf{G}}^{\tau}$ does not depend on the modulation type. This makes the test statistic $T_{\hat{\mathbf{G}}_r^{\tau}}$ and detection threshold $\psi_{\hat{\mathbf{G}}_r^{\tau}}$ independent of modulation too.

Fig. 7 presents the effect of the signal-to-interference ratio (SIR) on the average probability of correct identification $\mathrm{P_c}$ versus SNR. As shown in Fig. 7, it can be seen that the performance of the proposed algorithm improves by increasing SIR under the same conditions. This is mainly due to the fact that the received signal is less affected by the alpha stable interference when the value of SIR is large. In other words, when the value of SIR is larger, the peak characteristics of the discriminant matrix $\tilde{\mathbf{V}}_{\mathbf{G}}^{\tau}$ are more significant, so as to achieve a good identification performance for STBC-OFDM signals.

In the previous simulation, we assumed that timing synchronization and carrier synchronization are accurate. Fig. 8 shows the influence of the frequency offset Δf on the average probability of correct identification $\mathrm{P_c}$. We consider the normalized carrier frequency offset to the sub-carrier spacing of STBC-OFDM signals. As shown in Fig. 8, it can be seen that the performance of the proposed algorithm is affected by the frequency offset Δf. With Δf increasing, the performance of the proposed algorithm deteriorates, and when $\Delta f > 10^{-5}$, the performance degrades significantly. These results indicate that the generalized cross-correntropy features lack robustness for the frequency offset when the value of Δf is large.

Fig. 9 depicts the influence of the sample timing offset δ_Δ on the average probability of correct identification $\mathrm{P_c}$. As shown in Fig. 9, it can be seen that the performance of the proposed algorithm degrades by increasing the sample timing offset δ_Δ. This is because the generalized cross-correntropy is affected by sample timing offset δ_Δ. Especially, when $\delta_\Delta > 2$,

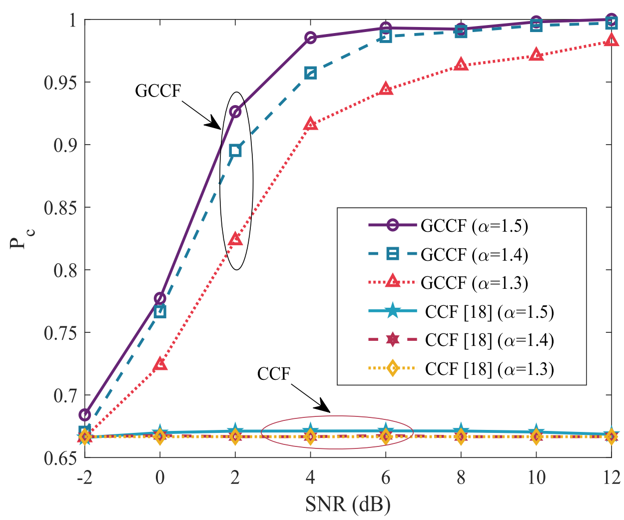

Fig. 10. The average probability of correct identification of the STBC-OFDM signals versus SNR, with different α values.

the peak characteristics of the generalized cross-correntropy is damaged significant to degrade identification performance for STBC-OFDM signals.

Fig. 10 shows the effect of the characteristic exponent α on the average probability of correct identification $\mathrm{P_c}$. A comparison with the algorithm based on cross-correlation function (CCF) in [18] is also included. According to Fig. 10, it can be seen that the proposed algorithm performance improves when the value of α increases. For $\mathrm{SNR} = 2\mathrm{dB}$, the average probability of correct identification $\mathrm{P_c}$ decreases from 0.96 to 0.82 when the characteristic exponent decreases from 1.5 to 1.3. Note from Fig. 10 that, by comparing the CCF algorithm and the proposed algorithm based on the generalized cross-correntropy function (GCCF), the proposed algorithm outperforms the CCF algorithm in symmetric alpha stable interference. This fact illustrates that the proposed algorithm is more robust to the symmetric alpha stable interference. Meanwhile, the main computational complexities of the proposed and existing algorithms are evaluated. When the number of observed blocks and receive antennas are N_b and M_r, the calculation complexity for GCCF estimator is $O\left(2M_rN_b\right)$ and the CCF estimator also have order $O\left(M_rN_b\right)$. As a result, the proposed algorithm achieves significant performance gain at the expense of increasing calculation complexity.

V. Conclusion

The blind identification algorithm based on a novel generalized cross-correntropy function for STBC-OFDM signals over frequency-selective fading channels has been proposed. The generalized cross-correntropy feature of the received signal from antenna pairs has been used by taking advantage of the space-time redundancy. The proposed algorithm used a strongly-distinguishable discriminating matrix to develop a decision tree scheme for identifying the STBC-OFDM signals. This algorithm has the advantage of avoiding the requirement for a priori information, such as modulation type, channel coefficients, signal-to-noise ratio, and interference power. Theoretical analysis and simulation have demonstrated that the proposed algorithm can achieve a good identification performance in the presence of impulsive interference, and is relatively robust with respect to the characteristic exponent, modulation type and signal-to-interference ratio. Future work includes developing a robust identification scheme for STBC-OFDM signals to tackle the influences of timing and frequency offsets, and exploring identification scheme in multi-user cases.

References

[1] Y. A. Eldemerdash, O. A. Dobre, and M. Oner, “Signal identification for multiple-antenna wireless systems: achievements and challenges,” *IEEE Commun. Surv. Tuts.*, vol. 18, no. 3, pp. 1524-1551, 3rd Quart. 2016.

[2] D. Zhang, Y. Lu, Y. Li, W. Ding and B. Zhang, “High-order convolutional attention networks for automatic modulation classification in communication,” *IEEE Trans. Wireless Commun.*, vol. 22, no. 7, pp. 4600-4610, Jul. 2023.

[3] M. Marey and O. A. Dobre, “Automatic identification of space-frequency block coding for OFDM systems,” *IEEE Trans. Wireless Commun.*, vol. 16, no. 1, pp. 117-128, Jan. 2017.

[4] Z. Chen, “A weight extreme value detection method of radio frequency I/Q data component for software-defined radio electromagnetic spectrum dynamic access strategy,” *IEEE Trans. Instrum. Meas.*, vol. 73, pp. 1-12, 2024.

[5] P. Ghasemzadeh, M. Hempel, H. Wang and H. Sharif, "GGCNN: an efficiency-maximizing gated graph convolutional neural network architecture for automatic modulation identification,” *IEEE Trans. Wireless Commun.*, vol. 22, no. 9, pp. 6033-6047, Sept. 2023.

[6] H. Moulay, A. B. Djebbar and B. Dehri, “Blind digital modulation classification for cooperative STBC-OFDM systems based on random subspace and adaBoost classifiers,” in *Proc. IEEE ISPA*, 2022, pp. 1-5.

[7] M. Gao, Y. Li, O. A. Dobre, and N. Al-Dhahir, “Joint blind identification of the number of transmit antennas and MIMO schemes using gerschgorin radii and FNN,” *IEEE Trans. Wireless Commun.*, vol. 18, no. 1, pp. 373-387, Jan. 2019

[8] M. Gao, Y. Li, O. A. Dobre and N. Al-Dhahir, “Blind identification of SFBC-OFDM signals using subspace decompositions and random matrix theory,” *IEEE Trans. Veh. Technol.*, vol. 67, no. 10, pp. 9619-9630, Oct. 2018.

[9] M. Gao, Y. Li, O. A. Dobre and N. Al-Dhahir, “Blind identification of SFBC-OFDM signals based on the central limit theorem,” *IEEE Trans. Wireless Commun.*, vol. 18, no. 7, pp. 3500-3514, Jul. 2019.

[10] V. Choqueuse, M. Marazin, L. Collin, K. C. Yao, and G. Burel, “Blind recognition of linear space-time block codes: a likelihood-based approach,” *IEEE Trans. Signal Process.*, vol. 58, no. 3, pp. 1290-1299, Mar. 2010.

[11] M. Marey, O. A. Dobre and H. Mostafa, “Cognitive radios equipped with modulation and STBC recognition over coded transmissions,,” *IEEE Wireless Commun. Lett.*, vol. 11, no. 7, pp. 1513-1517, Jul. 2022.

[12] V. Choqueuse, K. Yao, L. Collin, and G. Burel, “Hierarchical spacetime block code recognition using correlation matrices,” *IEEE Trans. Wireless Commun.*, vol. 7, no. 9, pp. 3526-3534, Sep. 2008.

[13] M. Marey, O. A. Dobre, and B. Liao, “Classification of STBC systems over frequency-selective channels,” *IEEE Trans. Veh. Technol.*, vol. 64, no. 5, pp. 2159-2164, May 2015.

[14] Y. A. Eldemerdash, M. Marey, O. A. Dobre, G. Karagiannidis, and R. Inkol, “Fourth-order statistics for blind classification of spatial multiplexing and alamouti space-time block code signals,” *IEEE Trans. Commun.*, vol. 61, no. 6, pp. 2420-2431, Jun. 2013.

[15] M. Shi, Y. Bar-Ness, and W. Su, “STC and BLAST MIMO modulation recognition,” in *Proc. IEEE GLOBECOM*, 2007, pp. 3034-3039.

[16] M. Marey, O. A. Dobre, and R. Inkol, “Classification of space-time block codes based on second-order cyclostationarity with transmission impairments,” *IEEE Trans. Wireless Commun.*, vol. 11, no. 7, pp. 2574-2584, Jul. 2012.

[17] M. Mohammadkarimi and O. A. Dobre, “Blind identification of spatial multiplexing and Alamouti space-time block code via kolmogorov smirnov (K-S) test,” *IEEE Commun. Lett.*, vol. 18, no. 10, pp. 1711-1714, Oct. 2014.

[18] M. Marey, O. A. Dobre, and R. Inkol, “Blind STBC identification for multiple-antenna OFDM systems,” *IEEE Trans. Commun.*, vol. 62,no. 5, pp. 1554-1567, May 2014.

[19] Y. A. Eldemerdash, O. A. Dobre, and B. J. Liao, "Blind identification of SM and alamouti STBC-OFDM signals," *IEEE Trans. Wireless Commun.*, vol. 14, no. 2, pp. 972-982, Feb. 2015.
[20] M. Marey, H. Mostafa, S. A. Alshebeili and O. A. Dobre, "STBC recognition for OFDM transmissions: channel decoder aided algorithm," *IEEE Commun. Lett.*, vol. 26, no. 7, pp. 1658-1662, Jul. 2022.
[21] E. Karami and O. A. Dobre, "Identification of SM-OFDM and AL-OFDM signals based on their second-order cyclostationarity," *IEEE Trans. Veh. Technol.*, vol. 64, no. 3, pp. 942-953, Mar. 2015.
[22] A. Sikri, B. Selim, G. Kaddoum, M. Au and B. L. Agba, "RIS-aided wireless sensor network in the presence of impulsive noise and interferers for smart-grid communications," *IEEE Commun. Lett.*, vol. 27, no. 9, pp. 2501-2505, Sept. 2023.
[23] U. Ashraf and G. R. Begh, "Effect of impulsive noise on IRS-aided communication systems," *IEEE Trans. Veh. Technol.*, vol. 72, no. 1, pp. 648-653, Jan. 2023.
[24] J. Zhang et al., "Blind parameter estimation of M-FSK signals in the presence of alpha-stable noise," *IEEE Trans. Commun.*, vol. 68, no. 12, pp. 7647-7659, Dec. 2020.
[25] M. Liu, Y. Han, Y. Chen, H. Song, Z. Yang and F. Gong, "Modulation parameter estimation of LFM interference for direct sequence spread spectrum communication system in alpha-stable noise," *IEEE Syst. J*, vol. 15, no. 1, pp. 881-892, March 2021.
[26] D. Lin, P. Chiang, and H. Li, "Performance analysis of two-branch transmit diversity block-coded OFDM systems in time-varying multipath rayleigh-fading channels," *IEEE Trans. Veh. Technol.*, vol. 54, no. 1, pp. 136-148, Jan. 2005.
[27] J. Li, D. Z. Feng and W. X. Zheng, "A robust decision directed algorithm for blind equalization under α-stable noise," *IEEE Trans. Signal Process.*, vol. 69, pp. 4949-4960, Jul. 2021.
[28] Y. Zhang and Y. Zhang, "An adaptive parameter estimation algorithm of radar linear frequency modulation signal based on nonlinear transform under different alpha stable distribution noise environments," *IEEE J. Miniaturization Air Space Syst.*, vol. 4, no. 4, pp. 389-399, Dec. 2023.
[29] X. Dong, M. Sun, J. Zhao, X. Zhang and Y. Wang, "Enhanced BNC approach for noncircular signals direction finding with sparse array in the scenario of impulsive noise," *IEEE Trans. Aerosp. Electron. Syst.*, vol. 59, no. 5, pp. 6265-6277, Oct. 2023.
[30] L. Gois, R. Suyama, D. Fantinato and A. Neves, "Relationship between criteria based on correntropy and second order statistics for equalization of communication channels," *IEEE Signal Process. Lett.*, vol. 29, pp. 1317-1321, May 2022.
[31] T. Liu, T. Qiu and S. Luan, "Cyclic frequency estimation by compressed cyclic correntropy spectrum in impulsive noise," *IEEE Signal Process. Lett.*, vol. 26, no. 6, pp. 888-892, Jun. 2019.
[32] J. Ma and T. Qiu, "Automatic modulation classification using cyclic correntropy spectrum in impulsive noise," *IEEE Wireless Commun. Lett.*, vol. 8, no. 2, pp. 440-443, Apr. 2019.